ACS Combinatorial Science

Research Article

pubs.acs.org/acscombsci

Search for New Catalysts for the Oxidation of SO_2

J. Loskyll, K. Stöwe, and W. F. Maier*

Technische Chemie, Universität des Saarlandes, 66123 Saarbrücken, Germany

Supporting Information

ABSTRACT: The focus of this paper is the search and characterization of novel catalysts for the gas phase oxidation of concentrated SO_2 for the production of sulfuric acid. Modern high-throughout (HT) methods such as emissivity corrected Infrared Thermography (ecIRT) and automated synthesis techniques were used for the synthesis and activity measurements of the samples. In addition a plug flow reactor that uses UV−vis online analytics for the quantification of the SO_2 conversion was designed, built and used for validation of the HT results. The study started with a highly diverse search space of elemental compositions designed for potential discovery. About a thousand samples were synthesized using sol−gel recipes and screened for catalytic SO_2 oxidation activity over a temperature range of 330−450 °C. Several novel catalyst systems were discovered during the screening process and the most interesting systems were further characterized. The most important doping effects on activity found were the influence of bismuth and selenium doping on standard sulfuric acid catalysts, the activity gain of chromium based catalysts caused by the doping with antimony and the activity gain of chromium as well as iron and vanadium based catalysts caused by the doping with tin.

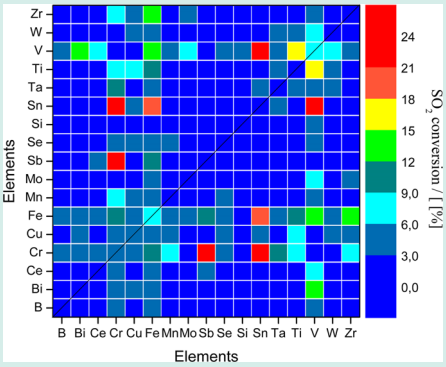

KEYWORDS: *heterogeneous catalysis, SO_2 oxidation, sulfuric acid production, high-throughput, emissivity corrected infrared thermography (ecIRT)*

1. INTRODUCTION

Sulfuric acid, with an annual production volume of about 200 Mt sulfuric acid, of which the largest part is produced by means of the contact process, is one of the most important products of the chemical industries.[1] Because of thermodynamics, SO_3-production would still benefit from catalysts which operate at lower temperature, so a search for such catalysts is still attractive.[2] In correspondence with the significance of the contact process a vast amount of research has been conducted on process and plant design as well as on catalyst composition, preparation and support materials. Nevertheless, with the exception of some minor optimizations (cesium doping, carrier stability and form, vanadium content, resistivity versus wet process gas)[2] the alkaline doped vanadium catalyst used in most industrial plants has remained unchanged since the BASF has patented the system in 1913.[3] Only for some niche applications other catalyst systems like noble metal based catalysts[4−9] or iron based catalysts (for high temperature processes)[10,11] are used or at least discussed. [For a more general overview regarding the current research efforts in sulfuric acid catalysis and the mechanism of the catalyzed SO_2 oxidation see the introduction of our review article from 2011.[12]] Whereas almost exclusively one catalyst system is used in industrial applications, the scientific and patent literature mentions plenty of additional systems, support materials, and modifications of the systems used. An overview of the elements mentioned in the literature is summarized in Scheme 1. For clarity reasons only one function (as base element, dopant or support material) and only one literature reference was assigned to each element, even if for some of them hundreds of references can be found.

As support materials, for example, asbestos,[29] Al_2O_3,[17] TiO_2 (anatase),[20] SiO_2,[17] diatomaceous earth,[17] MgF_2,[16] zeolite,[30] CPG (Controlled pore glass silica),[6] or activated carbon[15] are discussed. It is even for experts nearly impossible to judge the relative significance of the many potential catalysts, since results have been obtained in different laboratories at non standardized conditions, so direct comparison of data may be meaningless. Herein we present the results of a HT study, where data on numerous catalysts have been obtained under identical conditions and are such comparable.

We show, how a vast amount of elemental combinations can be synthesized and screened for their catalytic activity with the help of high-throughput (HT) methods. We also provide some insight into the best catalysts discovered and investigated. Herein catalysts are named as follows: a sample named $Cr_{75}Sb_{25}O_x$ has been prepared by mixing 75 molar parts of chromium and 25 molar parts of antimony precursor solutions. After the calcinations a mixed oxide of unknown oxidation states is formed. The oxygen content of the oxide was not determined independently. As it may also vary with oxygen partial pressure, pretreatment, temperature and under reaction conditions it is labeled O_x.

Received: February 19, 2013
Revised: June 18, 2013
Published: July 9, 2013

Scheme 1. Periodic Table of Elements for the SO_2 Oxidation

Ia	IIa	IIIb	IVb	Vb	VIb	VIIb	VIIIb			Ib	IIb	IIIa	IVa	Va	VIa	VIIa	VIIIa
H																	-
Li^{13}	Be^{14}											-	C^{15}	N	O	F^{16}	-
Na^{17}	Mg^{18}											Al^{17}	Si^{17}	P^{19}	S	-	-
K^{17}	Ca^{17}	-	Ti^{20}	V^{17}	Cr^{20}	Mn^{17}	Fe^{20}	Co^{19}	Ni^{19}	Cu^{21}	Zn^{19}	Ga^{22}	-	-	-	-	-
Rb^{23}	Sr^{16}	Y^{22}	Zr^{19}	Nb^{20}	Mo^{20}	-	Ru^{4}	Rh^{7}	Pd^{7}	Ag^{17}	-	In^{22}	Sn^{17}	Sb^{24}	Te^{17}	-	-
Cs^{25}	Ba^{17}	L^{22}	-	-	W^{20}	Re^{20}	Os^{26}	Ir^{27}	Pt^{7}	Au^{26}	-	-	Pb^{17}	Bi^{28}	-	-	-
-	-	A															

L^{22}	La^{22}	Ce^{19}													Yb^{27}	
A	-	-	-	U^{27}	-	-	-	-	-	-	-	-	-	-	-	-

Base element
Dopant
Support material

2. RESULTS AND DISCUSSION

2.1. HT Synthesis Design and ecIRT Screening. The starting point of the screening was a literature search for elements known to be catalytically active or to have a promoting effect in SO_2 oxidation catalysis. The results of this search are summarized in Scheme 1.

From the elements mentioned in the literature some were excluded (Os, Pm, U), others were added to the screening approach (B, Ge, Hf, Sc, Se, Ta) because of the availability of suitable precursors or being of interest because of analogy conclusions. As the number of elemental combinations for the 63 base elements proposed would have been too high (1953 binary or 39711 ternary oxides), a preselection was carried out.

Binary oxides ABO_x (ternary compounds):

$$\binom{n}{2} = \frac{n!}{2!(n-2)!} = 1953$$

Ternary oxides $ABCO_x$ (quarternary compounds):

$$\binom{n}{3} = \frac{n!}{3!(n-3)!} = 39711$$

In a first approach, the screening therefore started with binary and ternary oxide mixtures of Al, Co, Cr, Cu, Fe, Mn, Mo, Nb, Ni, Ta, Ti, and Zr synthesized by the sol−gel route of Wessler et al.[31] that had already been tested in our laboratory for stability in 1 M sulfuric acid solution in an earlier study.[32]

Following the initial ecIRT screening (results see below), the syntheses of the most interesting candidates together with vanadium pentoxide were repeated and also doped with 2 and 10 mol % of the elements Ag, Al, Au, B, Ba, Bi, Ca, Cd, Ce, Co, Cr, Cs, Cu, Dy, Er, Eu, Fe, Ga, Gd, Ge, Hf, Ho, In, Ir, K, La, Li, Lu, Mg, Mn, Mn, Mo, Na, Nb, Nd, Ni, Pb, Pd, Pr, Pt, Rb, Re, Rh, Ru, Sb, Sc, Se, Si, Sm, Sn, Sr, Ta, Tb, Te, Ti, Tm, V, W, Y, Yb, Zn, and Zr. The doped mixed oxides of this second generation were then studied by ecIRT.

It is well-known from literature that catalysts activities depend on synthesis parameters. Thus, in a second approach ternary oxides of B, Bi, Ce, Cr, Cu, Fe, Mn, Mo, Sb, Se, Si, Sn, Ta, Ti, V, W, and Zn and binary oxides of Bi, Ce, Cr, Fe, Sb, Si, and V were resynthesized using a different sol−gel synthesis route based on a publication of Chen et al. al.[33] and also screened for activity by ecIRT (see below). Active components identified were synthesized again and doped with 2 and 10 mol % of the elements Ca, Cs, Ga, Ge, K, Li, Mg, Na, Nb, Rb, and Zn.

The basic principle of ecIRT method is that exothermic reactions are accompanied by an evolution of heat ($\Delta H^0(SO_2 + {}^1/_2O_2 \rightarrow SO_3) = -100$ kJ mol^{-1}).[34] Therefore, the more active a catalyst for the conversion of SO_2 is, the higher is the amount of heat emitted by a catalyst. This heat of reaction can be detected by the IR camera as a temperature increase with spatial resolution (see also Figure 1). Of crucial importance for high temperature resolution is here the correction for surface emissivity as outlined in various publications before. The ecIRT method, its general applications, advantages and drawbacks were detailed in a recent review article.[35] The technology developed as well as the applicability of the ecIRT method for investigation of SO_2 oxidation catalysis was already subject of another publication.[12] Therefore most details of the technology applied here are given in ref 12.

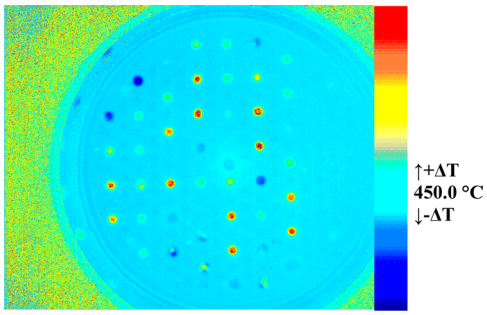

Figure 1. IR image of a catalyst library containing vanadium bismuth catalysts at 450 °C in an atmosphere consisting of 5 mL/min SO_2 and 50 mL/min air. The color bar indicates the temperature (emission) changes measured by the IR-camera (+6 to −4 °C). Details regarding composition and experimental procedures can be found in ref 12 and references therein.

The first generations did not result in new catalyst systems but were very helpful to validate the method.[36,37] It revealed that with the setup we were able to find several active catalyst systems that are already known in the literature. The results of the first generations may be summarized as follows: (i) V, Fe, and Cr show a low activity for the oxidation of SO_2 that decreased in the sequence V > Fe > Cr (less than 10% conversion at 450 °C see also section 2.3.2), (ii) the activity of vanadium based catalysts increased when they are doped with alkaline oxides, and (iii) noble metals like platinum increased the catalytic activity of SO_2 oxidation catalysts. 5% Pt on alumina reaches nearly equilibrium conversion at temperatures >400 °C.

dx.doi.org/10.1021/co400023j | ACS Comb. Sci. 2013, 15, 464−474

The results of the second approach are summarized in Figure 2 in section 2.2.

2.2. Conventional Validation. The contour diagram shown in Figure 2 visualizes the results of the conventional screening of the oxide catalysts of the second generation. One can clearly see that Cr, Fe, and V are the active elements, and while they show no inherent activity, Sn and Sb are the most interesting dopants. Also Bi, Ti, and Zr may be promising dopants. The screening of the binary oxides did not bring up new promising materials. Because of the results of the screening, the binary oxide systems Cr−Sb, Cr−Sn, Fe−Sn, and V−Sn were investigated in detail (see below). Here it should be mentioned, that porous mixed oxides are prone to deviations in microstructure originating from different relative amounts of crystalline and amorphous phases, which may be affected by experimental conditions, but also by seasonal changes of humidity, temperature and batches of precursors. The general trends reported here are reproducible, as documented by the performance of catalysts of related composition and error bars.

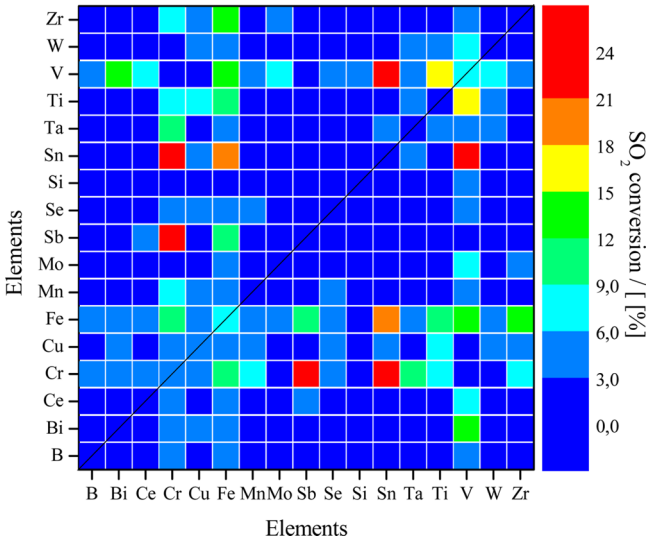

Figure 2. Diagram showing the conversion as a function of the elemental combination. The diagram has been diagonally mirrored. All measurements were made under identical conditions.

2.3. New Systems Discovered and Their Characterization. All systems discovered were characterized using single point physisorption, XRD and XRF analyses. They were synthesized using the sol−gel-route of Chen et al.[33] with the exception of the bismuth and selenium doped vanadium catalysts (section 3.1.3 and ref 28); the conversions measured were obtained at 450 °C under identical conditions in a plug flow reactor (see section 3.2).[12] Under our standard conditions, the best catalyst discovered achieved a conversion of 48%, the best vanadium-free catalyst achieved a conversion of 35% at 450 °C (our V-based industrial reference catalyst achieved a conversion of 62% at 450 °C). The industrial reference catalyst was a state of the art catalyst used here only as a standard to compare our materials to. Its absolute performance can not be commented on, since our reaction conditions are typical laboratory conditions, which have not been calibrated on industrial testing conditions.

2.3.1. Oxide System Cr−Sb. Two systems that showed some similarities to the Cr−Sb system discovered during our HTS can be found in the literature: the first is a diatomaceous earth supported chromium(VI) system containing about 4% of antimony that was synthesized using impregnation techniques and high pressure (280 °C; 200 atm)[24] and the second is a $Fe_7Cr_2Sb_4O_x$ system, that was reported to show activity at elevated temperatures of 600−650 °C in mixtures of SO_2 and pure O_2.[38]

The mixed oxides showed good activity with a maximum at a composition of $Cr_{72.1}Sb_{27.9}O_x$ (XRF analysis $Cr_{73(1)}Sb_{27(1)}O_x$) which is very close to the formal composition $Cr_{3/4}Sb_{1/4}O_2$. In Figure 3 the catalyst activity increases with Sb until it drops a

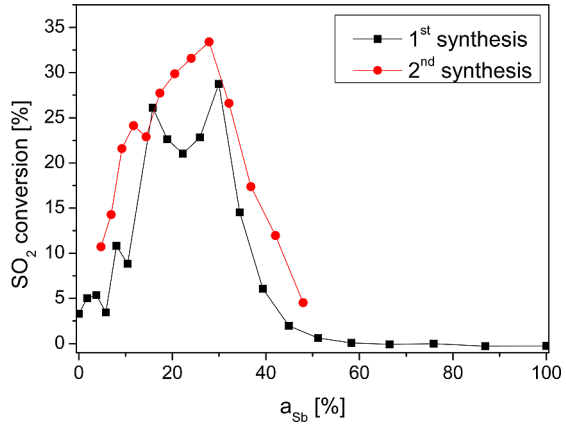

Figure 3. SO_2 conversion in the system $Cr_{100-a}Sb_aO_x$ as a function of *a*. The synthesis was repeated because no distinct maximum was located during the first screening.

little around 20% Sb content. To clarify the range of maximal conversion the composition range of interest has been resynthesized. In contrast to the first synthesis, which was calcined in an oven in the presence of many other catalysts, this time only the Cr−Sb-catalysts were calzined (it was assumed, that volatility of components from other catalysts may have contaminated the catalysts of the first synthesis). It was promising to see, that the activity trend across the SB-content was well reproduced and this time the conversion passed through a true maximum at a SB-content around 30 mol %. The exact location of the maximum is subject to some small deviations due to the partial volatility of $SbCl_5$ used for the synthesis (white deposits at the rim of the synthesis vessels and contamination of antimony-free samples that were placed in the same oven chamber during the calcination).

The doping with antimony clearly increased the specific surface areas of the catalysts. While the BET surface of Cr_2O_3 was only about S_{BET} = 8 m^2/g, the mixed oxides had surface areas S_{BET} > 130 m^2/g (see Table 1). Because of the known sublimation tendency of Sb_2O_4, the specific surface area of this sample was not measured, but the properties of the sample (visual appearance, crystallinity, and low heat of absorption of SO_2) indicate that the specific surface area is very small.

In the powder X-ray diffraction (PXRD) patterns of the oxide system Cr−Sb the change of phases is clearly visible. $Sb_{100}Cr_0O_x$ consists of highly crystalline orthorhombic cervantite (α-Sb_2O_4, ICSD no. 4109). $Sb_0Cr_{100}O_x$ can be identified as trigonal eskolaite (Cr_2O_3, ICSD no. 33642). The eskolaite phase shows several splitted reflections indicating a distortion of the unit cells resulting in a reduction of the crystal symmetry (see Supporting Information for details). It might be that this effect is caused by the traces of antimony detected

dx.doi.org/10.1021/co400023j | ACS Comb. Sci. 2013, 15, 464−474

Table 1. Composition, Chlorine Content, and Specific Surface Area in the Oxide System Cr−Sb[a]

composition (intended)	composition (XRF)	chlorine content (XRF) [%]	BET-surface area [m^2/g]
$Cr_{100}Sb_0O_x$	$Cr_{99.6(8)}Sb_{0.40(4)}O_x$	<0.2%	8
$Cr_{82.6}Sb_{17.4}O_x$	$Cr_{84(1)}Sb_{16.4(6)}O_x$	<0.2%	138
$Cr_{79.5}Sb_{20.5}O_x$	$Cr_{80(1)}Sb_{20.7(7)}O_x$	<0.2%	(232)
$Cr_{76.0}Sb_{24.0}O_x$	$Cr_{76(1)}Sb_{23.8(8)}O_x$	<0.2%	136
$Cr_{72.1}Sb_{27.9}O_x$	$Cr_{73(1)}Sb_{27.0(9)}O_x$	<0.2%	162
$Cr_{67.9}Sb_{32.1}O_x$	$Cr_{69(1)}Sb_{30.8(8)}O_x$	<0.2%	137
$Cr_0Sb_{100}O_x$	$Sb_{100(2)}O_x$	<0.2%	

[a]Second synthesis from Figure 3. The small antimony content of 0.4% found in the sample with the theoretic composition Cr_2O_3 shows that the antimony is partially volatile. The oven used for the calcinations contained a complete composition spread. The antimony found has migrated from the samples with a higher antimony content. The measured BET-surface area for $Cr_{79.5}Sb_{20.5}O_x$ was put into parentheses because of the low amount of substance used for the analysis, which results in a larger error.

during the XRF analysis of pure chromium oxide samples (see Table 1). Marked by arrows in the diagram is a tetragonal rutile-type $CrSbO_4$ (ICSD No. 108880) phase that is formed in the mixed oxide. Cr(VI) compounds like those described in the patent[24] mentioned above are not visible in the powder diffraction pattern. Also note that the PXRD pattern of Sb_2O_4 (shown in the Supporting Information) indicates that the system is phase pure. No significant amounts of antimony (oxide) chlorides were found in XRD or XRF data (<0.2%), which is surprising when taking into account that $SbCl_5$ was used as the antimony precursor. In Table 1 the surface area of $Cr_{72.1}Sb_{27.9}O_x$ is 25 m^2/g larger that that of $Cr_{67.9}Sb_{32.1}O_x$ despite similar composition. Since this did not affect catalytic activity (Figure 3) and surface area does not correlate very well with activity, the reason for this change in surface area was not investigated.

2.3.2. Tin Doping of Chromium, Iron, and Vanadium Oxides. During the HTS it was found, that tin, whose oxides show no catalytic activity at all, have, when used as dopants, a positive influence on the activity of chromium as well as iron and vanadium oxides. Figure 5 shows the effect of tin doping on the three base element oxides. Plotted in each case is the activity of the pure oxides in comparison to the activity of the most active doped oxide. While the activity of the base oxides is − as expected − low and descending in the sequence V > Fe > Cr[20] in all three cases a considerable increase of the activity, that has as not yet been described in the literature, can be observed.

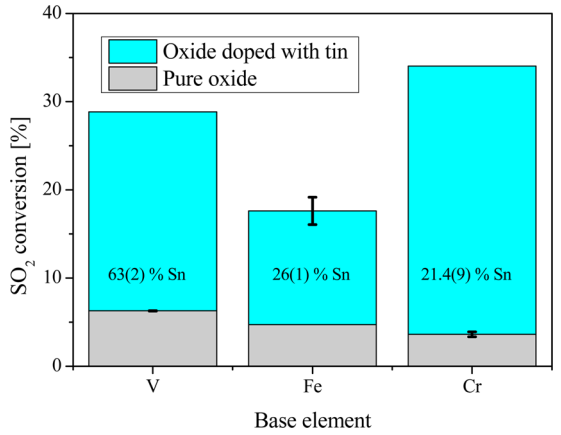

Figure 5. Influence of the Sn doping on the oxides of V, Fe, and Cr. In each case, the activity of the most active catalyst of a system is shown.

2.3.2.1. Oxide System Cr−Sn. In the system Cr−Sn (Figure 6) one can see, that even very small amounts of tin can considerably increase the activity. In contrast to the systems Fe−Sn and V−Sn, the activity maximum is rather broad/undefined and thus difficult to localize exactly. The most active Cr−Sn sample synthesized had a composition of $Sn_{39.3}Cr_{60,7}O_x$ ($Sn_{39(1)}Cr_{61(1)}O_x$ from XRF analysis) and reached a conversion of 31% at 450 °C. Figure 6 also indicates, that catalytic activity is not very dependent on catalyst composition in the range of 10−60% Sn. Important is, that the mixed oxides are much more active than the pure phases. This may have to do with a dramatic increase of amorphous phases and surface area, f.e. 1.9% of Sn increase the surface area by 540% as can be seen in

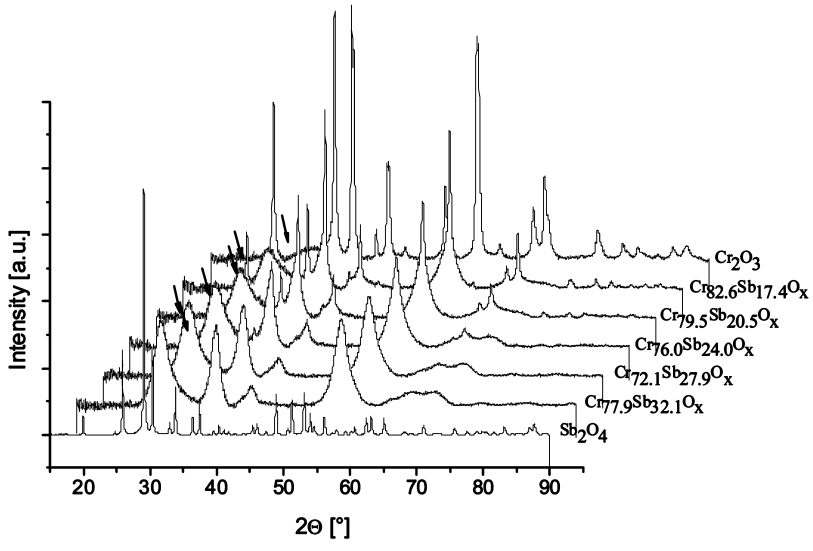

Figure 4. PXRD pattern of the oxide system Cr−Sb: The signal intensity of the pure Sb_2O_4 was scaled down by a factor of 10. Marked by arrows is the tetragonal rutile-type phase $CrSbO_4$ observed in the mixed oxides.

dx.doi.org/10.1021/co400023j | ACS Comb. Sci. 2013, 15, 464−474

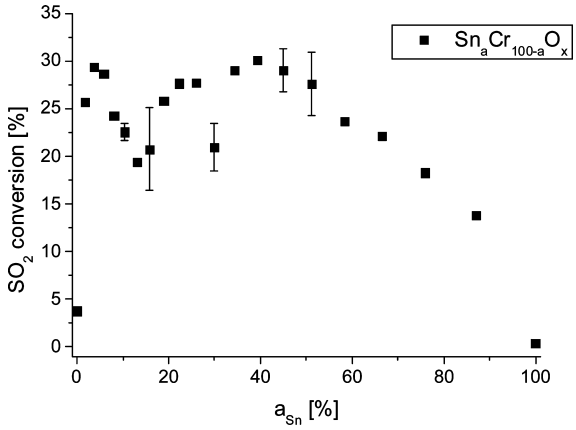

Figure 6. Conversion of the system $Sn_aCr_{100-a}O_x$ as a function of a_{Sn} at 450 °C.

Table 1. The pure Sn and Cr oxide phases tend to crystallize, which results in low surface area and activity.

Single-point BET physisorption measurements (Table 2) show that the doping with tin results in a significant increase of the specific surface area that correlates nearly linear with the percentage of tin in the mixed samples. The highest deviation between the elemental content determined by XRF analysis and that intended in synthesis is 1.5% (see Table 2). However, there is no good correlation of surface area with catalytic activity indicating that other factors contribute also. Additional characterization would be desirable to better understand the changes in activity.

Table 2. Composition and Specific BET Surface Area in the Oxide System Cr−Sb

composition (synthesis)	composition (XRF)	surface area [m^2/g]
$Sb_0Cr_{100}O_x$	$Sb_{0.4(4)}Cr_{99.6(8)}O_x$	8
$Sn_{1.8}Cr_{98.2}O_x$	$Sn_{1.9(2)}Cr_{98(1)}O_x$	51
$Sn_{3.7}Cr_{96.3}O_x$	$Sn_{3.9(2)}Cr_{96.1(9)}O_x$	76
$Sn_{5.8}Cr_{94.2}O_x$	$Sn_{5.7(4)}Cr_{94(1)}O_x$	94
$Sn_{13.0}Cr_{87.0}O_x$	$Sn_{12.9(6)}Cr_{87(1)}O_x$	131
$Sn_{18.9}Cr_{81.1}O_x$	$Sn_{21.4(9)}Cr_{79(1)}O_x$	147
$Sn_{34.4}Cr_{65.6}O_x$	$Sn_{33(1)}Cr_{67(1)}O_x$	208
$Sn_{39.3}Cr_{60.7}O_x$	$Sn_{39(1)}Cr_{61(1)}O_x$	239
$Sn_{44.9}Cr_{55.1}O_x$	$Sn_{44(2)}Cr_{56(2)}O_x$	257
$Sn_{100}Cr_0O_x$	$Sn_{100(2)}O_x$	61

In the PXRD pattern of the oxide system Cr−Sn (see Figure 7 and Supporting Information) all observed reflections can be assigned to tetragonal cassiterite (SnO_2, ICSD no. 55571) and trigonal eskolaite (Cr_2O_3, ICSD no. 33642). No formation of mixed oxide phases can be deduced from the diffraction patterns, only a line broadening accompanied by a decrease in signal intensity for both phases is visible on mutual doping.

2.3.2.2. Oxide System Fe−Sn. The system Fe−Sn showed a well-defined activity maximum (see Figure 8). The most active Fe−Sn sample synthesized has a composition of $Sn_{25.9}Fe_{74.1}O_x$ ($Sn_{26(1)}Fe_{74(1)}O_x$ from XRF analysis), which is close to a theoretical composition of $Fe_{3/2}Sn_{1/2}O_x$. This sample showed a conversion of 18% at 450 °C.

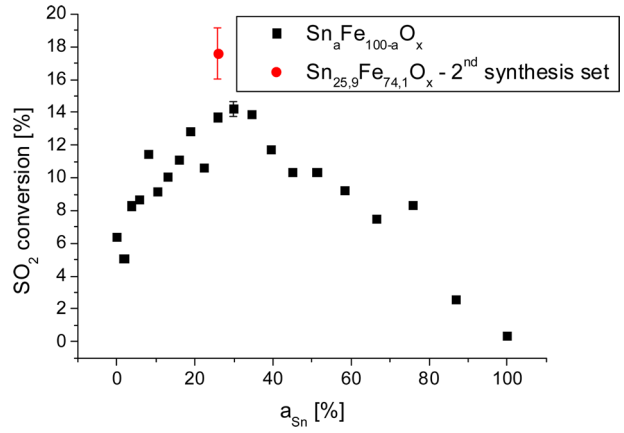

Figure 8. Conversion in the system $Sn_aFe_{100-a}O_x$ as a function of a_{Sn}.

As in the oxide system Cr−Sn the single-point BET physisorption measurements showed that the doping with tin resulted in a significant increase of the specific surface area. The highest deviation between the elemental content determined by XRF analysis and that intended in synthesis is again 1.5% (see Table 3).

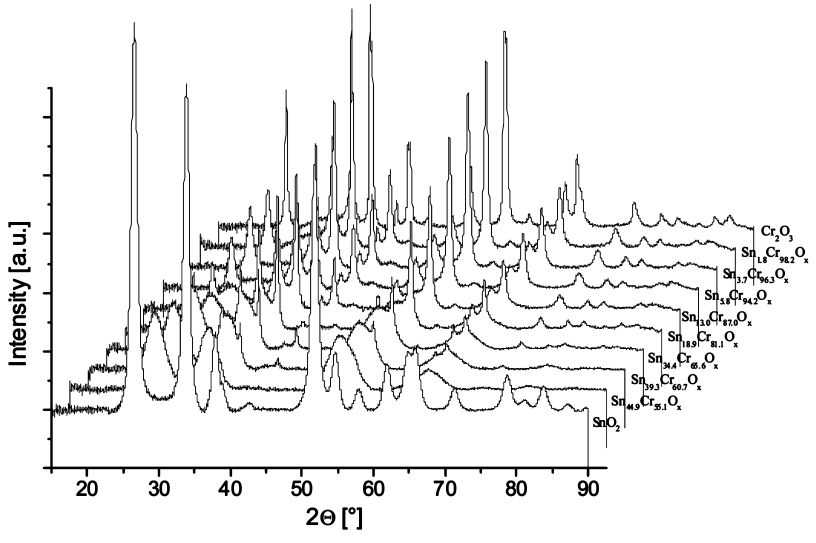

Figure 7. PXRD patterns of the oxide system Cr−Sn. The system is well-defined by ICSD references of trigonal Cr_2O_3 and tetragonal SnO_2.

dx.doi.org/10.1021/co400023j | ACS Comb. Sci. 2013, 15, 464−474

Table 3. Composition and Specific Surface Area in the Oxide System Fe−Sn

composition (intended)	composition (XRF)	BET surface area [m^2/g]
$Sn_0Fe_{100}O_x$	$Fe_{100.0(9)}O_x$	21
$Sn_{22.2}Fe_{77.8}O_x$	$Sn_{21.2(9)}Fe_{79(1)}O_x$	97
$Sn_{25.9}Fe_{74.1}O_x$	$Sn_{27.7}Fe_{72.3}O_x$	108
$Sn_{29.9}Fe_{70.1}O_x$	$Sn_{30(2)}Fe_{70(2)}O_x$	116
$Sn_{100}Cr_0O_x$	$Sn_{100(2)}O_x$	61
$Sn_{25.9}Fe_{74.1}O_x$, 2nd synthesis	$Sn_{26(1)}Fe_{74(1)}O_x$	205

During a second synthesis to optimize the calcination procedure a higher activity was measured for the $Sn_{25.9}Fe_{74.1}O_x$ sample. The single-point BET physisorption measurements showed that in the repeated synthesis a surface area nearly twice as large as in the first synthesis was achieved (see Table 3). The difference is also visible in the powder diffraction patterns. The second $Sn_{25.9}Fe_{74.1}O_x$ sample has a much lower crystallinity (see Figure 9).

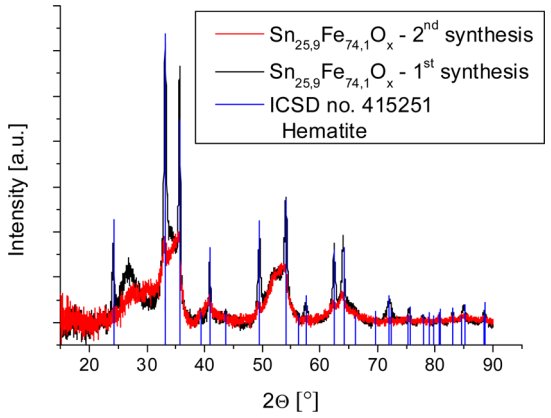

Figure 9. Comparison of the PXRD patterns of $Sn_{25.9}Fe_{74.1}O_x$ obtained during the 1st and 2nd synthesis and crystallographic phase assignment by ICSD reference of trigonal α-Fe_2O_3.

In the PXRD pattern of the system Fe−Sn, all reflection intensities can be described by tetragonal cassiterite (SnO_2, ICSD no. 55571) and trigonal hematite (α-Fe_2O_3, ICSD no. 415251). In the mixed oxides, a Rietveld refinement shows a shift of the lattice parameters of the SnO_2 phase indicating a doping of the SnO_2 phase with iron ($Sn_{100}Fe_0O_{x-a}$ = 4.7301(3) Å, c = 3.1812(2) Å; $Sn_{29.9}Fe_{70.1}O_x$ − a = 4.689(1) Å, c = 3.167(1) Å; $Sn_{22.2}Fe_{77.8}O_{x-a}$ = 4.652(2) Å, c = 3.179(2) Å). No shift in the lattice parameters of the hematite phase was observed.

2.3.2.3. Oxide System V−Sn. The system V−Sn shows a well-defined activity maximum (see Figure 11). The most active sample has a composition of $Sn_{65}V_{35}O_x$ ($Sn_{63(2)}V_{37(2)}O_x$ from XRF analysis). The highest conversion achieved was 28% at 450 °C.

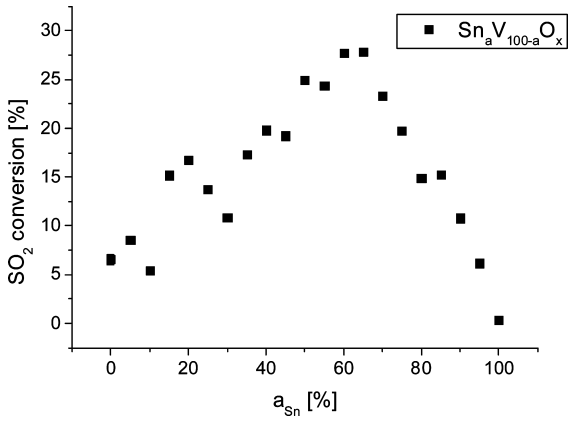

Figure 11. Conversion in the system $Sn_aV_{100-a}O_x$ as a function of a_{Sn}.

As in the two other systems physisorption measurements revealed that doping vanadium oxides with tin resulted in significant increases of the specific surface areas. The highest deviation between the elemental content determined by XRF analysis and that intended in synthesis is 2.8% (see Table 4).

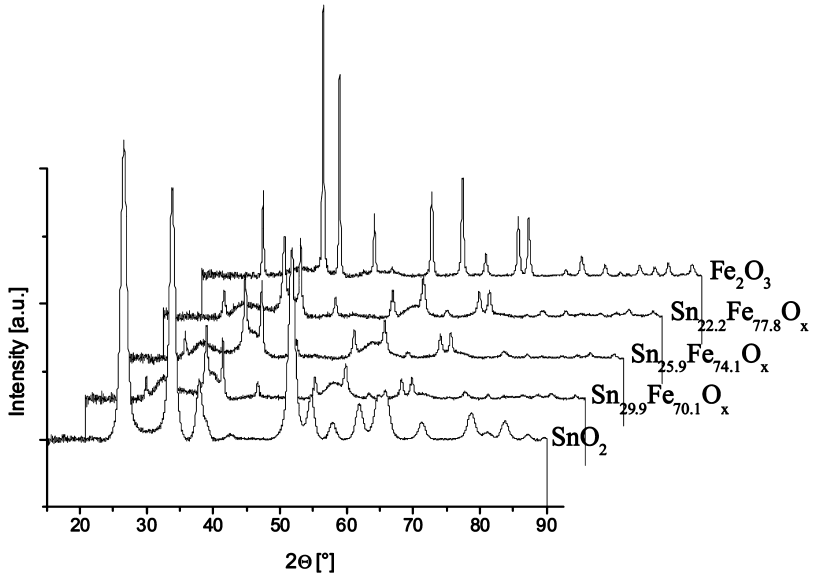

Figure 10. PXRD patterns of the oxide system Fe−Sn. All reflections can be explained by trigonal hematite and rutile-type cassiterite. For clarity the diffraction intensities of the SnO_2 phase was reduced by a factor of 3.

dx.doi.org/10.1021/co400023j | ACS Comb. Sci. 2013, 15, 464−474

Table 4. Composition and Specific Surface Area in the Oxide System V−Sn

composition (intended)	composition (XRF)	BET-surface area [m_2/g]
$Sn_0V_{100}O_x$	$V_{100(1)}O_x$	19
$Sn_{55}V_{45}O_x$	$Sn_{52(1)}V_{48(1)}O_x$	240
$Sn_{60}V_{40}O_x$	$Sn_{58(2)}V_{43(1)}O_x$	257
$Sn_{65}V_{35}O_x$	$Sn_{63(2)}V_{37(2)}O_x$	289
$Sn_{70}V_{30}O_x$	$Sn_{68(2)}V_{32(1)}O_x$	264
$Sn_{100}O_x$	$Sn_{100}O_x$	61

The PXRD patterns of the oxide system V−Sn are clearly affected by the diffraction pattern of the boundary phases (see Figure 12). The diffraction pattern of $Sn_0V_{100}O_x$ can be assigned to phase-pure shcherbianite (V_2O_5, ICSD no. 24042) and the sample $Sn_{100}V_0O_x$ to pure tetragonal cassiterite (SnO_2, ICSD no. 56671). The mixed oxides show a rutile-type tetragonal phase diffraction pattern of low crystallinity indicating a distortion of the cassiterite lattice in the presence of the doping element. A certain amount of the shcherbianite phase can be detected up to a composition of $Sn_{55}V_{45}O_x$.

2.4. Bismuth and Selenium Doping of Vanadium-Based Catalysts. Among the large number of feasible dopants two elements deserved special attention: Se and Bi. Selenides as active phases can be excluded in an oxidative environment, for selenium only oxoacid salts may play a role in catalysis. As the industrial sulfuric acid catalyst is vanadium based and supported on silicates together with an alkali metal pyrosulfate film, the influence of alkali metal selenates on the melting point and activity of the vanadium based catalysts was investigated. Bismuth is also of special interest as in a patent[28] a promoting effect of bismuth on vanadium based catalysts was reported.

2.4.1. Selenium Doping of Vanadium Based Catalyst. To dope vanadium−alkali metal based catalyst systems with selenium compounds goes back to a publication by Lapina et al. dealing with the structure determination of the active compound of the sulfuric acid catalyst. According to the authors the active phase of the sulfuric acid catalyst is a $[(V^VO)_2O(SO_4)_4]^{4-}$ ion that is part of a molten alkaline pyrosulfate layer formed on the catalyst support.[39] The ratio of the Na/K/Cs pyrosulfates and the amount of dissolved vanadium species hereby define the melting point of the active phase and thereby the lowest possible operation temperatures of the catalysts. Several publications have shown that a diverse range of compounds, in which sulfate has been (partially) substituted by selenate, do exist (for example $Na_xMe(1)^{II}_xMe(2)^{III}_{2-x}(SO_4)_{3-y}(SeO_4)_y$ (Me(1) = Mg, Zn, Cd, Mn, Me(2) = Al, Cr, Fe, In, Yb)[40] or $K[VO_2(SeO_4)(H_2O)_2]*H_2O$).[41] It is therefore conceivable that compounds of the type $[(V^VO)_2O(SO_4)_{4-x}(SeO_4)_x]^{4-}$ are stable in molten pyrosulfates/pyroselenates, lower the melting point of the mixture and catalyze the oxidation of SO_2.

For our studies, sodium and potassium selenate(VI) and hydrogen selenate(VI) containing compounds, such as $NaHSeO_4$, were synthesized by crystallization from H_2SeO_4 solutions as described by Brauer,[42] but instead of alkali metal carbonates hydroxides were used. Thermal analysis and titration showed that the compounds synthesized were not phase-pure but contained impurities of selenates(IV). Their influence on the performance of sulfuric acid catalysts was tested.

First we investigated the influence of the alkali metal selenate addition on the melting point of pyrosulfates. With the help of a TGA/DSC thermal analyzer, we measured the liquidus temperatures of the system $Na_xK_{2-x}S_2O_7$. The results correlate with the phase diagram measured by Rasmussen et al.[43] which was used as reference. However all solidification temperatures measured in our TGA/DSC were somewhat shifted to lower temperatures. This is probably caused by decomposition reactions ($Na_xK_{2-x}S_2O_7 \rightarrow Na_xK_{2-x}SO_4 + SO_3\uparrow$) that accompanied the melting and solidification process.

With the phase diagram of Rasmussen as a starting point $K_{1.2}Na_{0.8}S_2O_7$ and $K_{0.8}Na_{1.2}S_2O_7$ (the eutectic compositions[43]) were doped with $KHSeO_4$. We were able to show that the doping with selenates decreases the melting point of the mixtures. The best results were achieved with the doping of

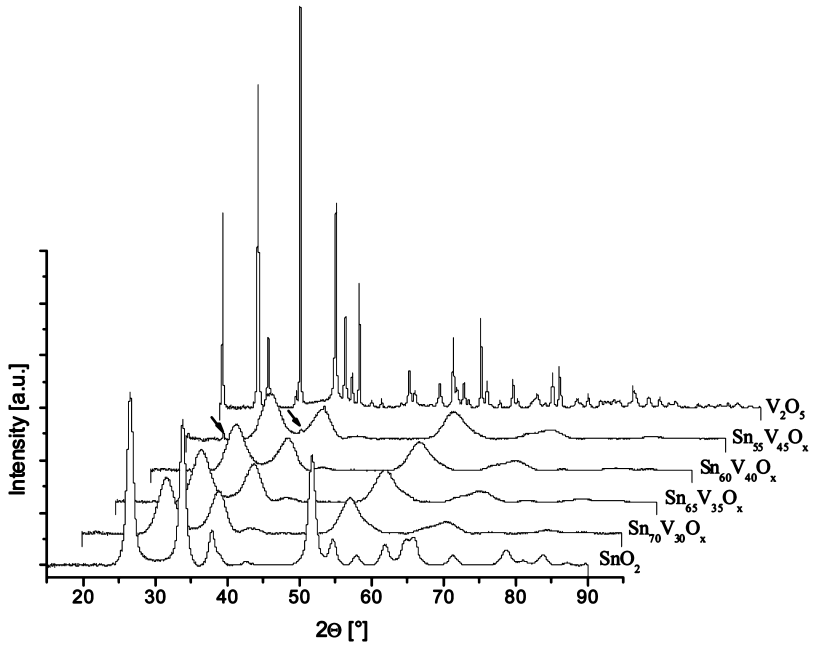

Figure 12. PXRD patterns of the oxide system V−Sn; remaining phase fraction V_2O_5 (shcherbianite) in $Sn_{55}V_{45}O_x$ is marked by arrows.

dx.doi.org/10.1021/co400023j | ACS Comb. Sci. 2013, 15, 464−474

$K_{1.2}Na_{0.8}S_2O_7$. At x_{Se} = 10 mol % the solidification temperature was decreased from 324 to 311 °C. As in the case of the pure pyrosulfates, the melting and solidification processes were accompanied by decomposition of the materials. SeO_2 from the samples condensed in the form of a white layer at the exhaust gas outlet of the TGA/DSC apparatus. This was confirmed by XRF analysis.

Subsequently, the effect of selenate doping on the activity of sulfuric acid catalysts was investigated. Two base vanadium catalyst mixtures, whose activities had been already confirmed by conventional measurements, were impregnated with different masses of $NaHSeO_4/KHSeO_4$ while keeping constant mass of the base catalysts. The resulting activities were compared with those of the base materials. No significant increase or decrease of the activities were observed. In all cases large quantities of red selenium condensed at the outlet of the plug flow reactors used for the measurements. Therefore no further experiments were conducted in this area.

2.4.2. Bismuth Doping of Vanadium Based Catalysts. In a patent of *Industrie Chimiche Dr. Baslini* from 1956 a huge positive effect of bismuth doping on the activity of vanadium based catalysts is described.[28] The catalysts were prepared by a mixed sol−gel and impregnation process involving water glass or diatomaceous earth, alkali vanadates, and bismuth dissolved in sulfuric acid. The patent data indicate that, especially the low temperature performance of the bismuth-doped catalysts, is by far superior to catalysts that contain only vanadium as an active component. Therefore catalysts were prepared according to the instructions given in the patent and a comparative study of the activities of doped and undoped catalysts was carried out.

The best catalyst of the silicate supported and sulfate promoted oxide system V−Bi prepared had a stable SO_2 conversion of 48% at 450 °C in the plug flow reactor, but in contrast to the patent specifications the performance at 390 °C is rather poor (7% conversion, see Figure 13). According to

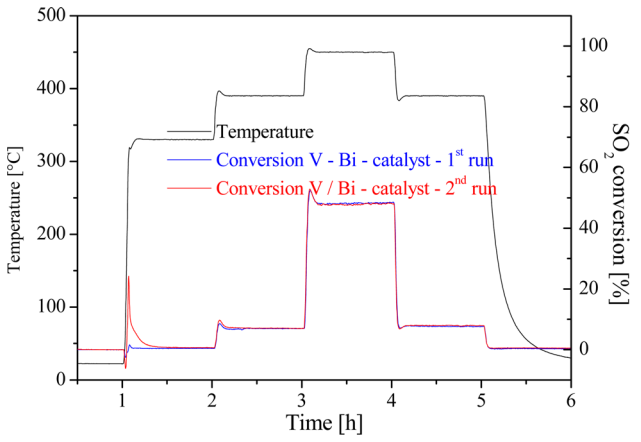

Figure 13. Determination of the conversion of the best catalyst of the silicate supported and sulfate promoted oxide system V−Bi. Shown are the initial measurement and a second reproduction run.

XRF analysis this catalyst had a molar composition of $Na_aK_5Si_{76.9}V_{13.8}Bi_{2.8}S_{1.5}O_x$. [The sodium content of the sample cannot be quantified using our RFA setup due to the low atomic weight of sodium.] PXRD reflections could be assigned to the two phases $NaBi_3V_2O_{10}$ (ICSD no. 88455) and $NaKV_2O_6$ (ICSD no. 82856). Broadness of reflections indicated a low crystallinity.

It was not unexpected that these systems, of whom the best is shown in Figure 13, show good catalytic activity; with vanadium as an active component, alkali metals as promoters and silicate as support these materials contain all components found in standard sulfuric acid catalysts plus bismuth. Because of this, we did not lay our focus on the optimization of the catalytic activity, but instead investigated the effect bismuth had on the catalytic activities of these materials. For this, we prepared materials that were synthesized by the same recipe under the same conditions (calcination in the same oven, identical aging time, etc.) but without BI content.

An example from this comparison is depicted in Figure 14, where a Bi−V catalyst (Bi/V = 0.66) is compared to the same

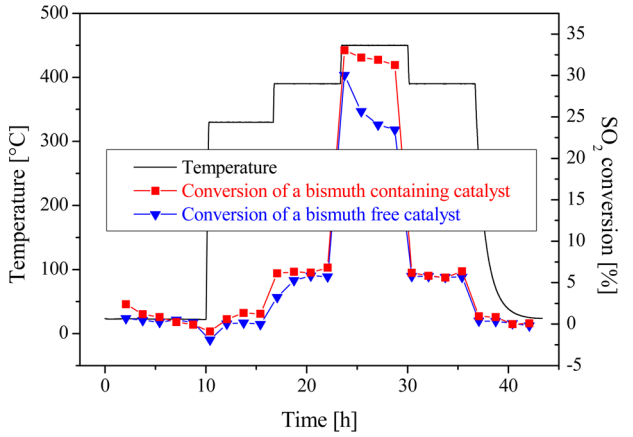

Figure 14. Activity comparison between Bi containing and Bi free vanadium catalysts. Except for the Bi content the synthesis conditions and elemental compositions were kept constant.

catalysts prepared without Bi. While the activities at the beginning are nearly the same for both systems, it can be seen that at 450 °C the activity of the bismuth free material is decreasing at a much faster rate than the activity of the Bi containing catalyst. From this we conclude that bismuth does not increase the activity of the fresh catalyst but stabilizes the catalyst. Even at 390 °C, the difference in activity between the two systems is negligible. The enhanced performances of the bismuth containing catalysts at low temperatures as proclaimed in the patent could not be reproduced in this study.

The systems based on water glass as support showed surface areas of ∼40 m^2/g. In contrast to this, standard sulfuric acid catalysts are based on diatomaceous earth as support and reveal surface areas of only 2−5 m^2/g This is sufficient for catalysis since the active catalyst is a molten film on the surface of the support.[44] This may indicate, that the water glass based systems are more susceptible to sintering than the standard sulfuric acid catalyst. Thus the bismuth added to the water glass supported catalysts may simply stabilize the microstructure.

3. EXPERIMENTAL SECTION

3.1. Syntheses. *3.1.1. Propionic Acid Based Sol−Gel Syntheses.* The propionic acid sol−gel syntheses based on a publication of Wessler et al.[31] used the following recipe: 1 mol metal precursor + 26.12 mol *i*-propanol + 25.20 mol propionic acid. In the following, the preparation is exemplified for an oxide material with the formal composition $Fe_{98}Mo_2O_x$:

Isopropanol and propionic acid were mixed 1:1 v/v; 1372 and 28 μL of 0.25 M solutions of $Fe(CH_3COO)_2$ and

dx.doi.org/10.1021/co400023j | ACS Comb. Sci. 2013, 15, 464−474

$Mo_2(CH_3COO)_4$, respectively, were stirred in an 1.5 mL GC vial. After the mixing, the solutions were placed in a fume hood for 2 days and subsequently in a drying oven at 40 °C for ten days, where they gelled. The calcination procedure was done in an oven. The temperature program consisted of a ramp of 30 °C/h, a 5 h plateau at 250 °C a second ramp and a second plateau at 400 °C. Afterwards, the oven was slowly cooled down. About 30 mg of metal oxide formed were crushed with a glass rod to give a fine powder. In Table S1 (Supporting Information), the elements used for the propionic acid based sol−gel synthesis and the corresponding precursors are listed. The dopants that have been separated from the base elements for clarity reasons are listed in Supporting Information Table S2. They were used to dope vanadium and iron based oxides with 2 and 10 mol %. The dopants were used in concentrations of 0.1 mol/L dissolved in methanol.

3.1.2. Ethylene Glycol Based Sol−Gel Route. This sol−gel route based on the publication by Chen et al.[33] used the following recipe: 1 mol metal precursor + 4 mol $HNO_{3,conc}$ + 37.5 mol H_2O + 18 mol ethylene glycol. The recipe is composition tolerant so that as metal precursors a wide range of nitrates, hydroxides, alkoxides, and chlorides can be used. In the following the preparation is exemplified for an oxide material with the formal composition $Fe_{50}Cr_{50}O_x$: HNO_3(65%), H_2O, and $(CH_2OH)_2$ were mixed 1/1.95/3.62 v/v and cooled down to room temperature. $Fe(NO_3)_3{\cdot}9H_2O$ and $Cr(NO_3)_3{\cdot}9H_2O$ were dissolved separately to give 0.548 M solutions. [The small volume expansion caused by the dissolution of the metal precursors was disregarded; when liquid precursors were used the volume expansion was taken into account.] Both stock solutions (2.5 mL) were mixed in 10 mL crimp neck vials and vigorously stirred. Gelling, drying, and calcination were all processed in an oven. At heating rates of 6 °C/h, the oven temperature was elevated to 80 °C and kept constant for 12 h. Afterwards, the temperature was raised to 105 °C at a rate of 6 °C/h and kept constant for 60 h. With a heating rate of 10 °C/h the temperature was elevated to 400 °C and kept constant for 5 h before the sample was cooled down again. About 200 mg of a mixed metal oxide was formed during the process.

In Table S3 (Supporting Information), the elements used for the ethylene glycol based sol−gel synthesis and the corresponding precursors were listed. The dopants were specified separately for clarity reasons in Table S3, they were used to dope $Sb_{25.9}Cr_{74.1}O_x$.

3.1.3. Water Glass Based Synthesis. The Bi-doped V oxide based catalysts were prepared according to a recipe of Greco et al. except that 20 mass % sulfuric acid (ice cooled) was used instead of concentrated sulfuric acid to dissolve Bi_2O_3.[28] For the second experiment, the batch solution was split into two parts and one-half was doped using bismuth stock solution. Chemicals used were potassium hydroxide [Merck], sodium silicate solution, sodium metavanadate [Aldrich, Sigma Aldrich], potassium metavanadate [Alfa Aesar] and concentrated sulfuric acid [Roth].

3.2. EcIRT Screening and Conventional Validation. The setup used for the conventional validations of the SO_2 conversions has been described in a prior publication.[12] The measurement principle is that the mixture of SO_2, and air is converted by constant masses of catalyst in a plug flow reactor. Downstream of the reactor the converted gas is stripped of SO_3 with the help of sugar absorber columns; the conversion is afterwards determined by measuring the SO_2 concentration of the off-gas. To further back up the results the mass balance was permanently monitored using a downstream mass flow meter. All conversion rates given in the text were measured under the following reaction conditions: (T = 450 °C; $V(SO_2)$ = 2 N mL/min; V(air) = 25 N mL/min; 100 mg catalyst diluted with 100 mg of SiO_2 (100−200 μm). For reference, the standard deviation of the conversion, measured by UV−vis spectroscopy at a SO_2 conversion of 46.6% in σ(c@X = 0.466), was ±1.9% (N = 5) indicating reliable validation results.

For details on the emissivity-corrected IR thermography high-throughput screening (HTS) method and the conventional validation of the HTS results in plug flow reactors see ref 12.

3.3. Single-Point Physisorption Data Aquisition. The physisorption measurements for the determination of the specific surface area of the sample were performed according to Brunauer, Emmett, and Teller by a single-point method (volume-axis intersection set to zero). About 200 mg of the samples were filled in glass burets and subsequently evacuated for 2 h at 200 °C. Afterwards, the weight was measured a second time. The physisorption measurements were carried out by a Sorpty 1750 instrument (Carlo Erba Instruments) using nitrogen as coolant and adsorbate.

3.4. Powder X-ray Diffraction (PXRD). The XRD measurements were performed by a X'Pert PRO diffractometer (PANalytical) that used Ni-filtered CuK_α radiation in Bragg−Brentano geometry and a variable divergence slit to keep the illuminated area constant. Steel discs with PMMA inlets were used as sample holders. The phase analysis was carried out using the software X'Pert HighScore Plus 2.2.3[45] that uses the Inorganic Crystal Structure Database (ICSD). For the Rietveld refinement, the software TOPAS 4.2 was used.[46]

3.5. X-ray Fluorescence Analysis (XRF). For the XRF analysis, pellets were pressed. 50 mg of each sample were filled in a piston press (Ø 4 mm; 2 tons; 1 min). The pellets were transferred into the sample chamber of a Eagle μProbe II spectrometer (Roentgenanalytik GmbH & Co. KG) that was evacuated for the analysis. The spectrometer used a rhodium anode at an excitation voltage of 40 kV. The sample analysis was conducted using the spectrometer software Vision 32 3.35.[47] All measurements were conducted trice. The error bar given in all tables is 3σ.

3.6. TGA/DSC. The device used for simultaneous thermal analysis was a TGA/DSC1 system (Mettler Toledo) equipped with high temperature oven HT1600, DTA FRS2 sensor and 70 μL platinum crucibles. Gas flow rates were adjusted using mass flow controllers (Bronkhorst). The DTA sensor was calibrated by adjusting the melting points and melting enthalpies of In, Zn, Al and Au at heating rates of 2, 5, 10, and 20 K/min at N_2 flow rates of 50 mL/min in 70 μL alumina crucibles. The sensitivity of the balance as a function of the temperature was checked using the decomposition of calcium oxalate monohydrate in a N_2 stream of 50 mL/min as a test reaction.

The melting points of the pyrosulfates and pyroselenates were determined by measuring the resolidification temperatures in dry nitrogen atmosphere. Twenty milligrams of substance mixtures were molten in 70 μL platinum crucibles placed in 120 μL alumina crucibles to avoid contamination of the DTA sensor. $Na_2S_2O_7$ and $K_2S_2O_7$ were synthesized by decomposition of the corresponding peroxodisulfates. Chemicals used were sodium peroxodisulfate, potassium peroxodisulfate, selenium dioxide, selenous acid, selenic acid (40% aq.) [Aldrich,

dx.doi.org/10.1021/co400023j | ACS Comb. Sci. 2013, 15, 464−474

Sigma Aldrich], and sodium and potassium hydroxide solutions [FIXANAL].

4. SUMMARY

The highly diverse high-throughput approach we used here to find new materials that are able to catalyze the oxidation of SO_2 was successful. In hundreds of measurements novel materials were screened for their SO_2 oxidation capability.

During the screening for binary oxide systems, the Cr−Sb oxides and positive influence of the elements Sn, Cr, Fe, and V on its ternary variations were discovered and confirmed in conventional measurements. Both systems were not previously described in the literature. While these systems are not on a par with state of the art industrial vanadium based catalysts, they show promising activity which may be further increased by proper optimization. Especially the doping of these catalysts with alkali metals and an optimization of the Sb−Sn−Cr oxide system seem worthwhile. A general problem of porous mixed oxides is the metal ion dependent trend to partial crystallization (defined phase formation). This affects the amorphous content as well as the porosity and is considered the main reason for experimental error and quantitative reproducibility of the catalysts.

Additional measurements in the patented oxide system Na/K−V−Bi gave new insights into the role of the bismuth compound. While the low temperature activity gain suggested in the patent literature was irreproducible the bismuth doping showed a stabilizing effect on the activity of the vanadium catalyst at elevated temperatures.

The selenate doping, while having no effect on the performance of sulfuric acid catalysts, did indeed decrease the melting point of pyrosulfate based mixtures that are the base of nearly all sulfuric acid catalysts currently in use.

■ ASSOCIATED CONTENT

Ⓢ Supporting Information

PXRD-patterns of the pure oxides and lists of the sol−gel precursors used. This material is available free of charge via the Internet at http://pubs.acs.org.

■ AUTHOR INFORMATION

Corresponding Author

*E-mail: wfmaier@online.de. Phone: +49/681/302/2422.

Notes

The authors declare no competing financial interest.

■ ACKNOWLEDGMENTS

The authors thank the Deutsche Forschungsgemeinschaft DFG for support through grant MA 1152/15-1, BASF SE for the reference catalyst and F. Rosowski, M. Kraemer, J. Zuehlke, and T. Lautensack for valuable discussions.

■ REFERENCES

(1) *Best Available Techniques Reference Document on the Production of Sulphuric Acid*; European Sulphuric Acid Association (ESA): Brussels, Belgium, 2000.

(2) Davenport, W. G.; King, M. G. *Sulfuric Acid Manufacture: Analysis, Control and Optimization*; Elsevier: Oxford, U.K., 2006.

(3) BASF Verfahren zur Herstellung einer Kontaktsubstanz zur Erzeugung von Schwefelsäureanhydrid. DE Patent DE000000291792A.

(4) Felthouse, T. R.; Bino, A. Ruthenium oxide catalysts for conversion of sulfur dioxide to sulfur trioxide. WO patent 2007/035949 A2, 2007.

(5) Kousopoulos, S.; Johannessen, T.; Eriksen, K. M.; Fehrmann, R. Titania-supported Pt and Pt−Pd nanoparticle catalyst for the oxidation of sulfur dioxide. *J. Catal.* **2006**, *238*, 206−213.

(6) Koutsopoulos, S.; Eriksen, K. M.; Fehrmann, R. Synthesis and characterization of supported Pt and Pt alloys nanoparticles used for the catalytic oxidation of sulfur dioxide. *J. Catal.* **2006**, *238*, 270−276.

(7) Koutsopoulos, S.; Rasmussen, S. B.; Eriksen, K. M.; Fehrmann, R. The role of support and promoter on the oxidation of sulfur dioxide using platinum based catalysts. *Appl. Catal., B* **2006**, *306*, 142−148.

(8) Pfeifer, P.; Zscherpe, T.; Haas-Santo, K.; Dittmeyer, R. Investigations on a Pt/TiO_2 catalyst coating for oxidation of SO_2 in a microstructured reactor for operation with forced decreasing temperature profile. *Appl. Catal., A* **2011**, *391*, 289−296.

(9) Benzinger, W.; Wenka, A.; Dittmeyer, R. Kinetic modelling of the SO_2-oxidation with Pt in a microstructured reactor. *Appl. Catal., A* **2011**, *397*, 209−217.

(10) Wiberg, N. *Holleman−Wiberg−Lehrbuch der Anorganischen Chemie*, 102 ed.; de Gruyter: Berlin, 2007.

(11) Wingen, A.; Anastasievic, N.; Hollnagel, A.; Werner, D.; Schueth, F. Fe-MCM-41 as a catalyst for sulfur dioxide oxidation in highly concentrated gases. *J. Catal.* **2000**, *193*, 248−254.

(12) Loskyll, J.; Stöwe, K.; Maier, W. F. High-throughput technology for novel SO_2 oxidation catalysts. *Sci. Technol. Adv. Mater.* **2011**, *12*, No. 054101/1−9.

(13) Vorlow, S.; Wainwright, M. S.; Trimm, D. L. The catalytic activity and selectivity of supported vanadia catalysts doped with alkali metal sulphates.: I. Structural re-organisations during pre-treatment and use. *Appl. Catal.* **2001**, *17*, 87−101.

(14) National Research Council. *Twelfth Report of the Committee on Catalysis*, National Research QD501 N35 1940 c.1; John Wiley and Sons Inc: New York, 1940; pp 166−168.

(15) Lee, J. K.; Hudgins, R. R.; Silveston, P. L. A cycled trickle-bed reactor for SO_2 oxidation. *Chem. Eng. Sci.* **1995**, *50*, 2523−2530.

(16) Stiles, A. B. The alkali earth salts as catalyst supports and stabilizers. *Catal. Today* **1992**, *14*, 269−276.

(17) Urbanek, A.; Trela, M. Catalytic-oxidation of sulfur-dioxide. *Catal. Rev.* **1980**, *21*, 73−133.

(18) Kuznetsova, S. M.; Dobkina, E. I.; Nefedova, L. A.; Lavrishcheva, S. A. Vanadium catalysts promoted with magnesium compounds for production of sulfuric acid. *Russ. J. Appl. Chem.* **2002**, *75*, 1816−1819.

(19) Dunn, J. P.; Stenger, H. G.; Wachs, I. E. Oxidation of sulfur dioxide over supported vanadia catalysts: molecular structure—Reactivity relationships and reaction kinetics. *Catal. Today* **1999**, *51*, 301−318.

(20) Dunn, J. P.; Stenger, H. G.; Wachs, I. E. Oxidation of SO_2 over supported metal oxide catalysts. *J. Catal.* **1999**, *181*, 233−243.

(21) Bogenstaetter, T.; Nickel J. T. Verfahren zur Herstellung von Schwefelsäure. WO patent 2009/060022 A1, 2009.

(22) Bhattacharyya, A. A.; Karch, J. A. Process for reducing emissions of sulfur oxides. EP patent 0 318 808 B1.

(23) Tandy, G. H. The role of alkali sulphates in vanadium catalysts for sulphur dioxide oxidation. *J. Appl. Chem.* **1956**, *6*, 68−74.

(24) Hund, F. Verwendung von Chromdioxid bzw. Chromdioxidmischphasen als Oxydationskatalysatoren. DE Patent 1252180.

(25) Doering, F. J.; Yuen, H. K.; Berger, P. A.; Unland, M. L. Investigation of the SO_2 oxidation rate limiting factors for K/V and Cs/V catalysts at low temperatures. *J. Catal.* **1987**, *104*, 186−201.

(26) Richards, A. K. Converting sulfur dioxide to sulfur trioxide in high-concentration manufacturing, using activated carbon with dopants and stripping. U.S. patent 2005/0287057 A1, 2005.

(27) Demmel, E. J.; Vierheilig, A. A.; Lippert, R. B. SOX additive systems based upon use of multiple particle species. CA patent 2302529.

(28) Greco, G. Improvements relating to the catalytic oxidation of sulphur dioxide to sulphur trioxide. GB patent 749,645.

(29) Knietsch, R. Ueber die schwefelsäure und ihre production nach dem contactverfahren. *Ber. Dtsch. Chem. Ges.* **1901**, *34*, 4069−4115.
(30) Wingen, A.; Anastasieviec, D.; Hollnagel, A.; Werner, D.; Schueth, F. Fe-MCM-41 as a novel sulfuric acid catalyst for SO_2 rich feeds. *Stud. Surf. Sci. Catal.* **2000**, *130*, 3065−3070.
(31) Wessler, B.; Jéhanno, V.; Rossner, E.; Maier, W. F. Combinatorial synthesis of thin film libraries for microwave dielectrics. *Appl. Surf. Sci.* **2004**, *223*, 30−34.
(32) Welsch, F. G.; Stoewe, K.; Maier, W. F. Rapid optical screening technology for direct methanol fuel cell (DMFC) anode and related electrocatalysts. *Catal. Today* **2011**, *159*, 108−119.
(33) Chen, C. C.; Nasrallah, M. M.; Anderson, H. U. Synthesis and Characterization of $(CeO_2)_{0.8}(SmO_{1.5})_{0.2}$ Thin Films from polymeric Precursors. *J. Electrochem. Soc.* **1993**, *140*, 3555−3559.
(34) Atkins, P. W. *Physikalische Chemie*, 5th ed.; Wiley-VCH Verlag GmbH: Weinheim, Germany, 2001.
(35) Loskyll, J.; Stoewe, K.; Maier, W. F. Infrared thermography as a high-throughput tool in catalysis research. *ACS Comb. Sci.* **2012**, *14*, 295−303.
(36) Loskyll, J. Untersuchungen zur Eignung der IR-Thermographie als Werkzeug zur Entdeckung neuer Sulfidkatalysatoren sowie als Werkzeug für die Suche nach neuen Katalysatoren für die SO_2-Oxidation. Diploma thesis, Saarland University, 2008.
(37) Loskyll, J. Suche nach neuen Katalysatoren für die Oxidation von SO_2. Dissertation, Saarland University, 2012.
(38) Sasaki, K.; Kizawa, Y.; Fukaya, K.; Yagi, H.; Voneyama, M. Improvement in the catalytic production of sulfuric acid. 6. Oxidation of sulfur dioxide with pure oxygen. *KGDKBU* **1975**, *13*, 54−73.
(39) Lapina, O. B.; Bal'zhinimaev, B. S.; Boghosian, S.; Eriksen, K. M.; Fehrmann, R. Progress on the mechanistic understanding of SO2 oxidation catalysts. *Catal. Today* **1999**, *51*, 469−479.
(40) Slater, P. R.; Greaves, C. Synthesis and conductivities of sulfate selenate phases related to nasicon—Naxm'(II)-Xm''(III)$_{2-x}(SO_4)_{3-y}(SeO_4)_y$. *J. Solid State Chem.* **1993**, *107*, 12−18.
(41) Tyutyunnik, A. P.; Krasil'nikov, V. N.; Berger, I. F.; Zubkov, V. G.; Perelyaeva, L. A.; Baklanova, I. V. Synthesis, structure, and physicochemical properties of $K[VO_2(SeO_4)(H_2O)]$ and $K[VO_2(SeO_4)(H_2O)_2]\cdot H_2O$. *Russ. J. Inorg. Chem.* **2011**, *56*, 1168−1177.
(42) Brauer, G., *Handbuch der präparativen anorganischen Chemie*, 3rd ed.; Ferdinand Enke Verlag: Stuttgart, Germany, 1975; p 425.
(43) Rasmussen, S. B.; Eriksen, K. M.; Hatem, G.; Da Silva, F.; Stahl, K.; Fehrmann, R. Conductivity, thermal measurements, X-ray investigations, and phase diagram of the $Na_2S_2O_7$-$K_2S_2O_7$ system. *J. Phys. Chem. B* **2001**, *105*, 2747−2752.
(44) Llyoyd, L. *Handbook of Industrial Catalysts*; Springer, New York, 2011.
(45) *X'Pert HighScore Plus 2.2.3*; PANalytical B. V.: Almelo, The Netherlands, 2007.
(46) *TOPAS, General Profile and Structure Analysis Software of Powder Diffraction Data*, version 4.2; Bruker AXS: Karlsruhe, Germany, 2003.
(47) *Vision 32 XRF-Software for Eagle II μ-Probe*, version 3.35; EDAX Inc.: Mahwah, U.S.A., 2002.